# SILICON ABUNDANCES IN NEARBY STARS FROM THE Si I INFRARED LINES[*]

J. R. Shi[1], M. Takada-Hidai[2], Y. Takeda[3], K. F. Tan[1], S. M. Hu[4], G. Zhao[1], and C. Cao[4]
[1] Key Laboratory of Optical Astronomy, National Astronomical Observatories, Chinese Academy of Sciences,
Beijing 100012, Peoples' Republic of China; sjr@bao.ac.cn
[2] Liberal Arts Education Center, Tokai University, 4-1-1 Kitakaname, Hiratsuka, Kanagawa 259-1292, Japan
[3] National Astronomical Observatory of Japan 2-21-1 Osawa, Mitaka, Tokyo 181-8588, Japan
[4] Shandong Provincial Key Laboratory of Optical Astronomy and Solar-Terrestrial Environment,
Shandong University at Weihai 264209, Peoples' Republic of China

## ABSTRACT

We have used high-resolution, high signal-to-noise ratio infrared spectra from the Subaru Telescope atop Mauna Kea. Line formation calculations of Si I infrared lines in the atmospheres of nearby stars are presented. All abundance results of [Si/Fe] are derived from local thermodynamic equilibrium (LTE) and NLTE statistical equilibrium calculations and spectrum synthesis methods. We found that NLTE effects for Si I infrared lines are important even for metal-rich stars ($>0.1$ dex), and the NLTE effects may depend on the surface gravities. A good agreement of silicon abundances between the optical and infrared lines is obtained when the NLTE effects are included, while a large difference is found for the LTE results. The derived silicon abundances are overabundant for metal-poor stars.

## 1. INTRODUCTION

Silicon is an important $\alpha$-capture element, the abundances of which play a key role in studying the Galactic chemical evolution. It is believed that silicon is created during oxygen and neon burning in massive stars (Woosley & Weaver 1995; Ohkubo et al. 2006); Type Ia supernove also produce significant amounts of silicon (Tsujimoto et al. 1995; Iwamoto et al. 1999; Thielemann et al. 2002; Maeda et al. 2010).

The previous abundance determinations of Si have been based on optical lines and the assumption of local thermodynamic equilibrium (LTE). For extremely metal-poor stars, the only optical lines at 3905 and 4103 Å can be used to determine Si abundances. Recently, it was found that the infrared Si I lines can also be observed (Jönsson et al. 2011) for metal-poor stars. However, we noted that the infrared lines are sensitive to the NLTE effects even in the solar spectrum (Shi et al. 2008). Thus, it is important to investigate the NLTE effects for these infrared lines in metal-poor stars.

The present work is based on a sample of nearby stars and aims at exploring their [Si/Fe] abundance ratios based on the Si I infrared lines, applying a full spectrum synthesis based on level populations calculated from the statistical equilibrium equations, and to investigate whether similar silicon abundances can be obtained from the infrared and optical lines. In Section 2, we present the observational technique and the atmospheric models, and stellar parameters are discussed in Section 3. NLTE line formation is discussed in Section 4. The results and comparison with those from the optical lines are given in Section 5. The discussion and conclusions are presented in Section 6.

## 2. OBSERVATIONS

The high-resolution spectra analyzed in our present investigation were obtained with the Infrared Camera and Spectrograph (IRCS; Kobayashi et al. 2000; Tokunaga et al. 1998) along with the 188-element curvature-based adaptive optics system (AO188), which is mounted on the IR Nasmyth focus of the 8.2 m Subaru Telescope atop Mauna Kea, on 2009 July 29 and 30 (UT). The observations cover a spectral range from 10100 to 11900 Å. The spectra were taken in the échelle spectrograph mode of IRCS, which is equipped with a Raytheon $1024 \times 1024$ InSb array with an Aladdin II multiplexer. The spectral resolution of $R$ is $\simeq 20{,}000$. All stars were observed with S/N $\sim$ 100–300.

For HD 131156, high-resolution and high signal-to-noise (S/N) optical spectra were obtained with the fiber optics échelle spectrograph attached to the 2.16 m telescope at the National Astronomical Observatories (Xinglong China) on 2011 August 3. The observations cover a spectral range from 3700 Å to 9200 Å. The spectra were exposed on a $4096^2$ CCD chip with $12\,\mu$m pixel size, providing a spectral resolving power of $R \sim 50{,}000$. It was observed six times with S/N $\sim$ 200.

Data extraction followed the standard "echelle" package of the software IRAF[5] including subtraction for background cancellation, flat fielding, bad-pixel correction, cosmic-ray events correction, scattered-light subtraction, aperture extraction, wavelength calibration, co-adding of spectrum frames, and continuum normalization (Takeda & Takada-Hidai 2011a, 2011b, for details).

## 3. METHOD OF CALCULATION

### 3.1. Model Atmospheres

We use line-blanketed LTE model atmospheres generated by Fuhrmann et al. (1997). As shown by Fuhrmann et al. (1993), this model is almost identical to the more widely

---

**Table 1**
Atomic Data of Silicon Infrared Lines[a]

| λ (Å)(Air) | Transition | $\log gf$ | $\log C_6$ | NLTE |
|---|---|---|---|---|
| 10288.90 | $4s\,^3P_0^o$–$4p\,^3S_1$ | −1.65 | −30.661 | −0.02 |
| 10371.30 | $4s\,^3P_1^o$–$4p\,^3S_1$ | −0.85 | −30.659 | −0.10 |
| 10585.17 | $4s\,^3P_2^o$–$4p\,^3S_1$ | −0.14 | −30.659 | −0.18 |
| 10603.45 | $4s\,^3P_1^o$–$4p\,^3P_2$ | −0.34 | −30.677 | −0.09 |
| 10627.66 | $4p\,^1P_1$–$4p\,^3P_2^o$ | −0.39 | −30.692 | −0.15 |
| 10661.00 | $4s\,^3P_0^o$–$4p\,^3P_1$ | −0.34 | −30.687 | −0.04 |
| 10689.73 | $4p\,^3D_1$–$4d\,^3F_2^o$ | −0.07 | −29.964 | −0.07 |
| 10694.27 | $4p\,^3D_2$–$4d\,^3F_3^o$ | +0.06 | −29.944 | −0.07 |
| 10727.43 | $4p\,^3D_3$–$4d\,^3F_4^o$ | +0.25 | −29.907 | −0.10 |
| 10749.40 | $4s\,^3P_1^o$–$4p\,^3P_1$ | −0.20 | −30.689 | −0.06 |
| 10784.57 | $4p\,^3D_2$–$4d\,^3F_2^o$ | −0.69 | −29.965 | −0.01 |
| 10786.88 | $4s\,^3P_0^o$–$4p\,^3P_0$ | −0.34 | −30.691 | −0.05 |
| 10827.10 | $4s\,^3P_2^o$–$4p\,^3P_2$ | +0.21 | −30.677 | −0.06 |
| 10843.87 | $4P\,^1P_1$–$4d\,^1D_2^o$ | −0.08 | −30.145 | −0.11 |
| 10882.83 | $4p\,^3D_3$–$4d\,^3F_3^o$ | −0.80 | −29.945 | −0.00 |
| 10979.34 | $4s\,^3P_2^o$–$4P\,^3P_1$ | −0.55 | −30.688 | −0.04 |

**Note.** [a] $\log gf$ values have been determined from NLTE solar spectrum fits, and damping constants $\log C_6$ for Si I infrared lines are computed according to the tables in Anstee & O'Mara (1991, 1995) and Barklem et al. (2000).

known model of Kurucz (1979). The main characteristics are: the iron opacity was calculated with the improved meteoritic value $\log \varepsilon_{\rm Fe} = 7.51$ (Anders & Grevesse 1989); opacities for metal-poor stars with [Fe/H] $< −0.6$ were calculated using $\alpha$-element abundances enhanced by 0.4 dex, and the mixing-length parameter $l/H_p$ was adopted to be 0.5, in order to determine consistent temperatures for H$_\alpha$ and the higher Balmer lines (Fuhrmann et al. 1993). Grupp (2004) discussed in detail our MAFAGS-OS and ODF models, and the differences from the MARCS and Kurucz models.

### 3.2. Stellar Parameters

We adopt the stellar parameters for the sample stars determined by Gehren et al. (2004, 2006) and Shi et al. (2004), where the effective temperatures are derived from the wings of the Balmer lines based on the hydrogen resonance broadening calculated with Ali & Griem's (1966) theory. The surface gravities are based on the HIPPARCOS parallaxes. Iron abundances are obtained from Fe II lines, and the microturbulence velocities are estimated by requiring that the iron abundance derived from Fe II lines should not depend on equivalent width. For G 29-23, fortunately, high-resolution and high S/N spectra covering a wide wavelength range were available from the archived ESO VLT/UVES (Dekker et al. 2005) spectra database. In order to keep our analysis consistent, for G 29-23 and HD 131156 we determined the stellar parameters using the method described above. The estimated uncertainties for the temperature, surface gravity, metal abundance, and microturbulence velocity are ±80 K, 0.10 dex, 0.05 dex, and 0.2 km s$^{-1}$, respectively, for most of the stars.

### 3.3. Atomic Line Data

Table 1 lists the relevant line data with their final solar NLTE fit values (Shi et al. 2008). Collisional broadening through van der Waals interaction with hydrogen atoms is important for infrared Si lines. The damping constants $\log C_6$ for Si I infrared lines are computed according to the table from Anstee & O'Mara (1991, 1995) and Barklem et al. (2000). Gehren et al. (2001, 2004) found that the values of the van der Waals

damping constants, such as Fe, Na, Mg, and Al, etc., can be best described by those calculated from the tables of Anstee & O'Mara (1991, 1995) and Barklem et al. (2000). In our analysis, the absolute value of the oscillator strengths is unimportant because the abundances are evaluated in a fully differential way with respect to the Sun.

## 4. NLTE CALCULATIONS

### 4.1. Atomic Model

The silicon model atom includes the most important levels of Si I and Si II and is comprised of 132 terms of Si I, 41 terms of Si II, plus the Si III ground state. As usual, the *level system* of silicon was extracted from the NIST data bank.[6] Silicon in cool stars is fully represented by the first three ionization stages, where for the purpose of NLTE calculations Si III reduces to the ground state, $3s^2\,^1S$. The atomic properties are documented in Shi et al. (2008, 2009).

*Line transitions* are based on the work of the Opacity Project (Seaton et al. 1994), in particular the calculations of Nahar & Pradhan (1993). The total number of lines included is 786 for Si I and 182 for Si II. For NLTE transfer calculations, simple Gauss profiles were used with nine wavelength points each.

*Bound–free transition* cross-sections with complex structure are available from calculations at the TOPbase[7] (see also Nahar & Pradhan 1993). The cross-sections of the lowest three terms, $3p\,^3P$, $3p\,^1D$, and $3p\,^1S$, are an order of magnitude greater than those of the next terms, which is very similar to the configuration of Mg (Zhao et al. 1998). It tends to decouple the metastable terms efficiently from the excited ones.

*Background opacities* are calculated with an opacity sampling code based on the hydrogen lines, the line lists made available by Kurucz (1992), and on the important bound–free cross-sections of hydrogen and the most abundant metals. The background opacities are sampled on a *random grid* of between 5000 and 10,000 wavelengths, to which are added the wavelengths of the line profiles. The final NLTE line formation program thus samples roughly 14,000 wavelengths. In the UV, where most of the background opacity is expected, the wavelength intervals of the random grid are between 1 and 4 Å. We emphasize that the choice of this frequency grid affects only the *bound–free* radiative interaction rates. In the earlier experiments with finer frequency mesh of up to 40,000 randomly sampled frequencies for Fe I, Gehren et al. (2001) showed that the influence of a very dense frequency sampling is less than marginal. This is similar to the sampling situation for OS model atmospheres, where changes in temperature corrections drop below a few Kelvin when the number of frequencies is increased to values beyond 10,000 (Grupp 2004, Figure 8). Background opacities for *bound–bound* transitions are sampled at the corresponding line frequencies.

*Inelastic collisions* with electrons and hydrogen atoms for both excitation and ionization are taken into account in our Si NLTE calculations. The formulae of van Regemorter (1962) and Allen (1973) are used to describe the excitation of allowed and forbidden transitions by electron collisions, respectively. Ionization cross-sections for electron collisions are calculated by applying the formula of Seaton (1962). Drawin's (1968, 1969) formula as described by Steenbock & Holweger (1984) is used to calculate neutral hydrogen collisions, with a similar

---

[6]   http://www.physics.nist.gov/
[7]   http://cdsweb.u-strasbg.fr/topbase/topbase.html
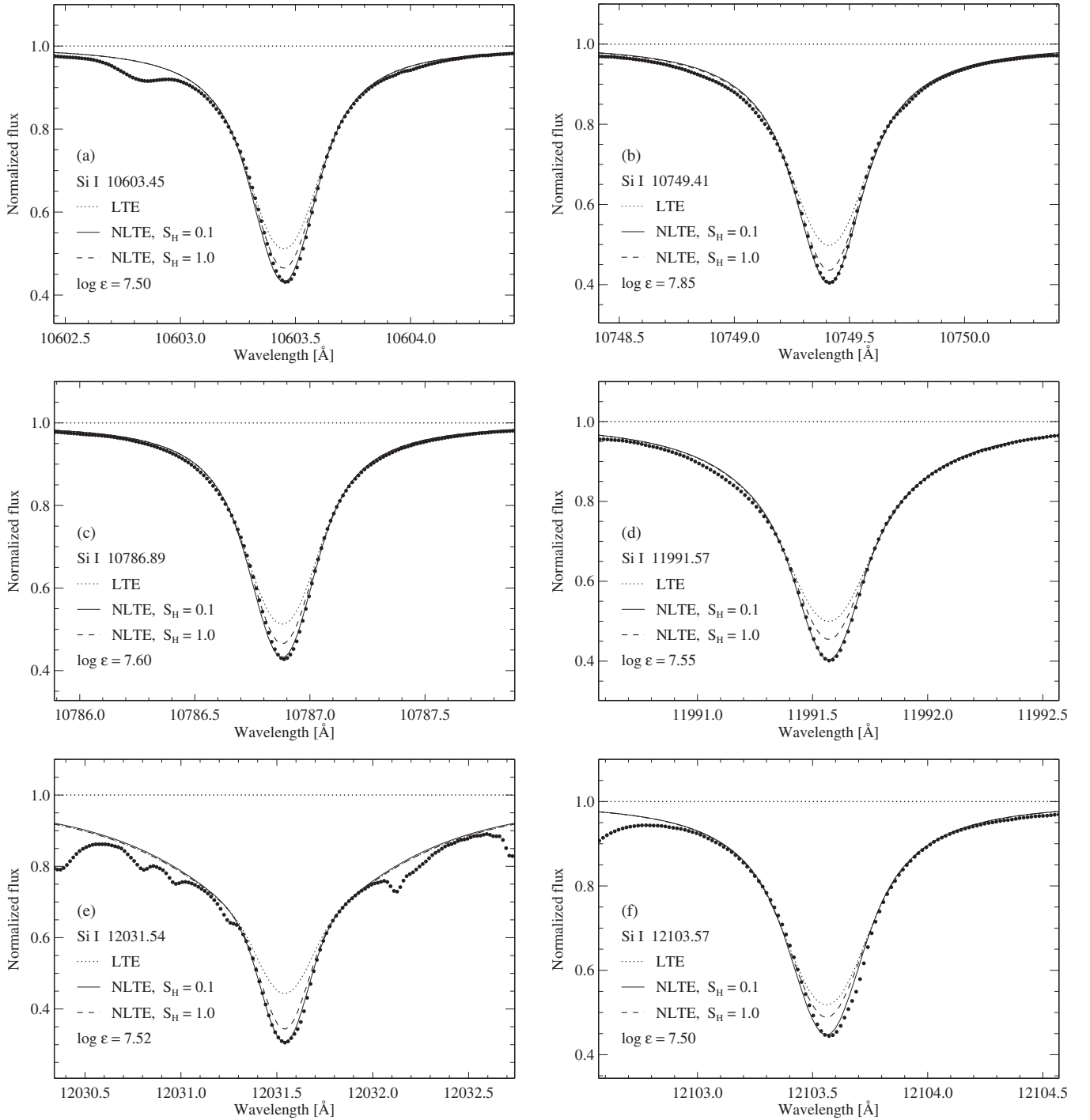
**Figure 1.** Near-infrared Si I solar line profiles. NLTE and LTE profiles are calculated for the same abundance, where the NLTE profile with $S_H = 0.1$ refers to the best fit.

formula for bound–free hydrogen collisions. To allow for some empirical correction to the Drawin approximations, a scaling factor $S_H$ is applied to the formula in our calculations.

The variation of the hydrogen collision scaling factor $S_H$ between 0 and 1 allows us to introduce changes similar to those resulting from electron collisions. Due to the large number of hydrogen atoms, the neutral hydrogen collision rates can be significantly stronger than the electron collision rates. For the Sun, in the range of $S_H$ parameters considered here, they do not lead to significant changes in the line profiles in the visible, where abundance differences for the two extremes ($S_H = 0$

and 1) stay within 0.03, . . . , 0.04 dex. This situation changes significantly, when the Si I near-infrared lines are analyzed. As evident from Table 1, most of these are absorbed from either $4s\,^3P^o$, $4p\,^1P$, or $4p\,^3D$. Since all the excited terms are only loosely coupled to each other and to other high-excitation terms, their departure coefficients tend to diverge from each other at $\log\tau \simeq -2$ (see Shi et al. 2008, Figure 4), i.e., where the cores of the relatively strong near-infrared lines form. This is the reason for the slightly increased abundance trend with the hydrogen collision scaling factor. For lines beyond $1\,\mu$m, the corresponding abundance variations can reach more
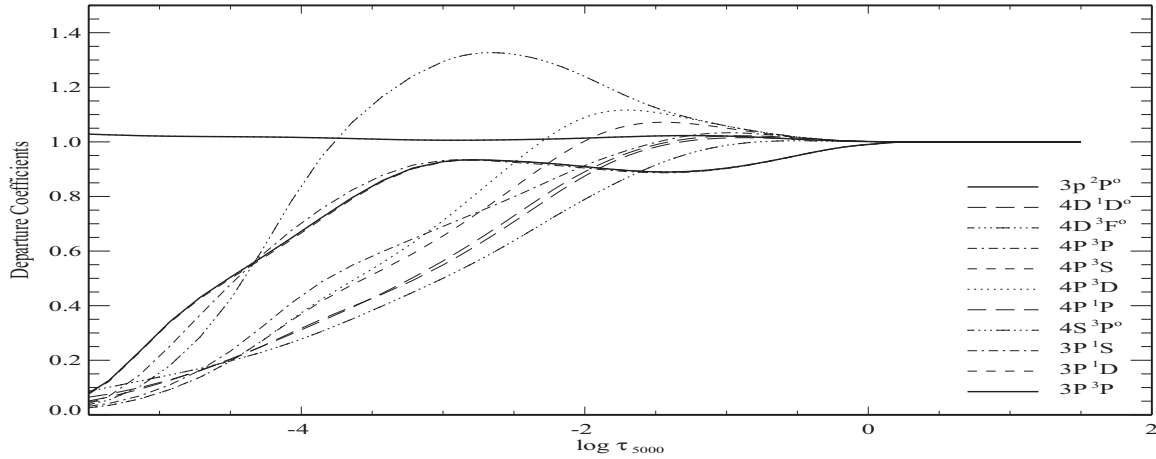
**Figure 2.** Departure coefficients as a function of log $\tau$ for selected levels of Si I and Si II ground state in the model atmosphere of HD 19445.

**Table 2**
Stellar Silicon LTE and NLTE (For Each Star, the First and the Second Rows, Respectively) Abundances Given
Relative to the Iron LTE Abundances Derived From the Fe II Lines ([Si/Fe])[a]

| Name | 10288 | 10371 | 10585 | 10603 | 10627 | 10661 | 10689 | 10694 | 10727 | 10749 | 10784 | 10786 | 10827 | 10843 | 10882 | 10979 |
|---|---|---|---|---|---|---|---|---|---|---|---|---|---|---|---|---|
| G 29-23 |  | 0.36 | 0.46 | 0.36 |  | 0.31 |  |  | 0.41 | 0.41 |  | 0.24 | 0.46 |  |  |  |
|  |  | 0.27 | 0.27 | 0.24 |  | 0.23 |  |  | 0.26 | 0.23 |  | 0.20 | 0.20 |  |  |  |
| HD 6582 | 0.30 | 0.36 | 0.49 | 0.38 | 0.33 | 0.36 | 0.38 | 0.36 | 0.40 | 0.39 | 0.30 | 0.32 | 0.46 | 0.34 | 0.33 |  |
|  | 0.30 | 0.32 | 0.38 | 0.29 | 0.28 | 0.29 | 0.34 | 0.31 | 0.32 | 0.32 | 0.30 | 0.28 | 0.31 | 0.27 | 0.32 |  |
| HD 10700 | 0.10 | 0.20 | 0.31 | 0.13 | 0.18 | 0.23 | 0.20 | 0.21 | 0.22 | 0.20 | 0.12 | 0.12 | 0.22 | 0.15 |  |  |
|  | 0.08 | 0.10 | 0.12 | 0.07 | 0.11 | 0.12 | 0.15 | 0.14 | 0.11 | 0.06 | 0.12 | 0.07 | 0.10 | 0.06 |  |  |
| HD 19445 |  | 0.33 | 0.28 | 0.24 | 0.28 | 0.23 |  | 0.23 |  | 0.40 |  | 0.24 | 0.36 |  |  |  |
|  |  | 0.28 | 0.20 | 0.19 | 0.26 | 0.18 |  | 0.22 |  | 0.28 |  | 0.18 | 0.18 |  |  |  |
| HD 122563 |  | 0.39 | 0.56 | 0.44 |  | 0.40 |  |  |  |  |  | 0.41 | 0.53 |  |  |  |
|  |  | 0.21 | 0.21 | 0.20 |  | 0.20 |  |  |  |  |  | 0.18 | 0.18 |  |  |  |
| HD 131156 | 0.04 | 0.19 | 0.24 | 0.11 | 0.06 | 0.16 | 0.14 | 0.14 | 0.11 | 0.11 | 0.04 | 0.11 | 0.12 | 0.06 |  | 0.10 |
|  | 0.02 | 0.09 | 0.10 | 0.05 | 0.03 | 0.09 | 0.09 | 0.08 | 0.03 | 0.03 | 0.03 | 0.06 | 0.08 | 0.01 |  | 0.08 |
| HD 140283 |  | 0.43 | 0.46 | 0.36 |  | 0.40 |  |  |  |  |  |  | 0.47 |  |  |  |
|  |  | 0.26 | 0.22 | 0.22 |  | 0.24 |  |  |  |  |  |  | 0.21 |  |  |  |
| HD 141004 | 0.06 | 0.19 | 0.14 | 0.12 | 0.09 | 0.16 | 0.20 | 0.20 | 0.20 | 0.12 | 0.03 | 0.12 | 0.19 | 0.19 |  |  |
|  | 0.05 | 0.08 | 0.09 | 0.06 | 0.00 | 0.05 | 0.06 | 0.09 | 0.06 | 0.02 | 0.01 | 0.02 | 0.08 | 0.08 |  |  |
| HD 142373 | 0.12 | 0.26 | 0.34 | 0.26 | 0.26 | 0.33 | 0.32 | 0.31 | 0.31 | 0.26 | 0.10 | 0.23 | 0.36 | 0.31 |  |  |
|  | 0.12 | 0.10 | 0.14 | 0.10 | 0.12 | 0.12 | 0.15 | 0.14 | 0.11 | 0.06 | 0.08 | 0.06 | 0.11 | 0.11 |  |  |
| HD 148816 |  | 0.39 | 0.40 | 0.36 | 0.35 | 0.44 | 0.41 | 0.40 | 0.40 | 0.42 |  | 0.38 | 0.40 |  |  |  |
|  |  | 0.27 | 0.30 | 0.26 | 0.28 | 0.25 | 0.29 | 0.26 | 0.28 | 0.26 |  | 0.26 | 0.26 |  |  |  |
| HD 161797 | 0.00 | 0.20 | 0.31 | 0.13 | 0.19 | 0.26 | 0.25 | 0.24 | 0.29 | 0.26 | 0.02 | 0.20 | 0.26 | 0.30 |  |  |
|  | 0.00 | 0.05 | 0.12 | 0.06 | 0.06 | 0.12 | 0.10 | 0.06 | 0.07 | 0.06 | 0.02 | 0.06 | 0.08 | 0.06 |  |  |
| HD 182572 | 0.21 | 0.35 | 0.31 | 0.31 | 0.26 | 0.34 | 0.28 | 0.26 | 0.25 | 0.24 | 0.18 | 0.18 | 0.31 | 0.24 |  |  |
|  | 0.21 | 0.21 | 0.22 | 0.16 | 0.14 | 0.20 | 0.19 | 0.16 | 0.16 | 0.16 | 0.15 | 0.14 | 0.14 | 0.13 |  |  |
| HD 194598 |  | 0.31 | 0.38 | 0.26 | 0.24 | 0.26 | 0.28 | 0.30 | 0.32 | 0.26 |  | 0.29 | 0.44 | 0.30 |  |  |
|  |  | 0.25 | 0.16 | 0.18 | 0.18 | 0.18 | 0.22 | 0.24 | 0.21 | 0.15 |  | 0.16 | 0.23 | 0.22 |  |  |
| HD 201891 |  | 0.46 | 0.50 | 0.40 | 0.39 | 0.38 | 0.38 | 0.46 | 0.45 | 0.38 |  | 0.40 | 0.49 |  |  |  |
|  |  | 0.36 | 0.31 | 0.30 | 0.34 | 0.31 | 0.33 | 0.36 | 0.35 | 0.29 |  | 0.29 | 0.30 |  |  |  |
| HD 224930 |  | 0.25 | 0.35 | 0.23 | 0.19 | 0.21 | 0.20 | 0.24 | 0.30 | 0.24 |  | 0.18 | 0.25 | 0.19 |  |  |
|  |  | 0.15 | 0.17 | 0.13 | 0.10 | 0.10 | 0.15 | 0.16 | 0.20 | 0.13 |  | 0.10 | 0.15 | 0.10 |  |  |

**Note.** [a] Our NLTE calculations for Fe I/II based on the advanced atomic model (Mashonkina et al. 2011) support the earlier conclusion of Korn et al. (2003) that the NLTE effects for the Fe II lines are negligible.

than 0.1 dex, and their cores suggest the choice of $S_H = 0.1$ (Figure 1).

All calculations are carried out with a revised version of the DETAIL program (Butler & Giddings 1985) using accelerated lambda iteration (see Gehren et al. 2001, 2004 for details).

### 4.2. NLTE Effects

Figure 2 shows the behavior of the departure coefficients $b_i = n_i^{\rm NLTE}/n_i^{\rm LTE}$ of the important levels of Si I and Si II ground

state as a function of continuum optical depth ($\tau_{5000}$ referring to $\lambda = 5000$ Å) in the model atmosphere of HD 19445. Here, $n_i^{\rm NLTE}$ and $n_i^{\rm LTE}$ are the statistical equilibrium and thermal (Saha–Boltzmann) number densities, respectively. We can see that the three lowest levels of Si I are underpopulated in the deep atmosphere, while the levels $4s\,^3P^o$ of Si I and Si II ground state are overpopulated in the line formation region due to the ionization cross-sections of the lowest three terms, $3p\,^3P$, $3p\,^1D$, and $3p\,^1S$, which are an order of magnitude greater than those of the next terms. It tends to efficiently decouple the metastable
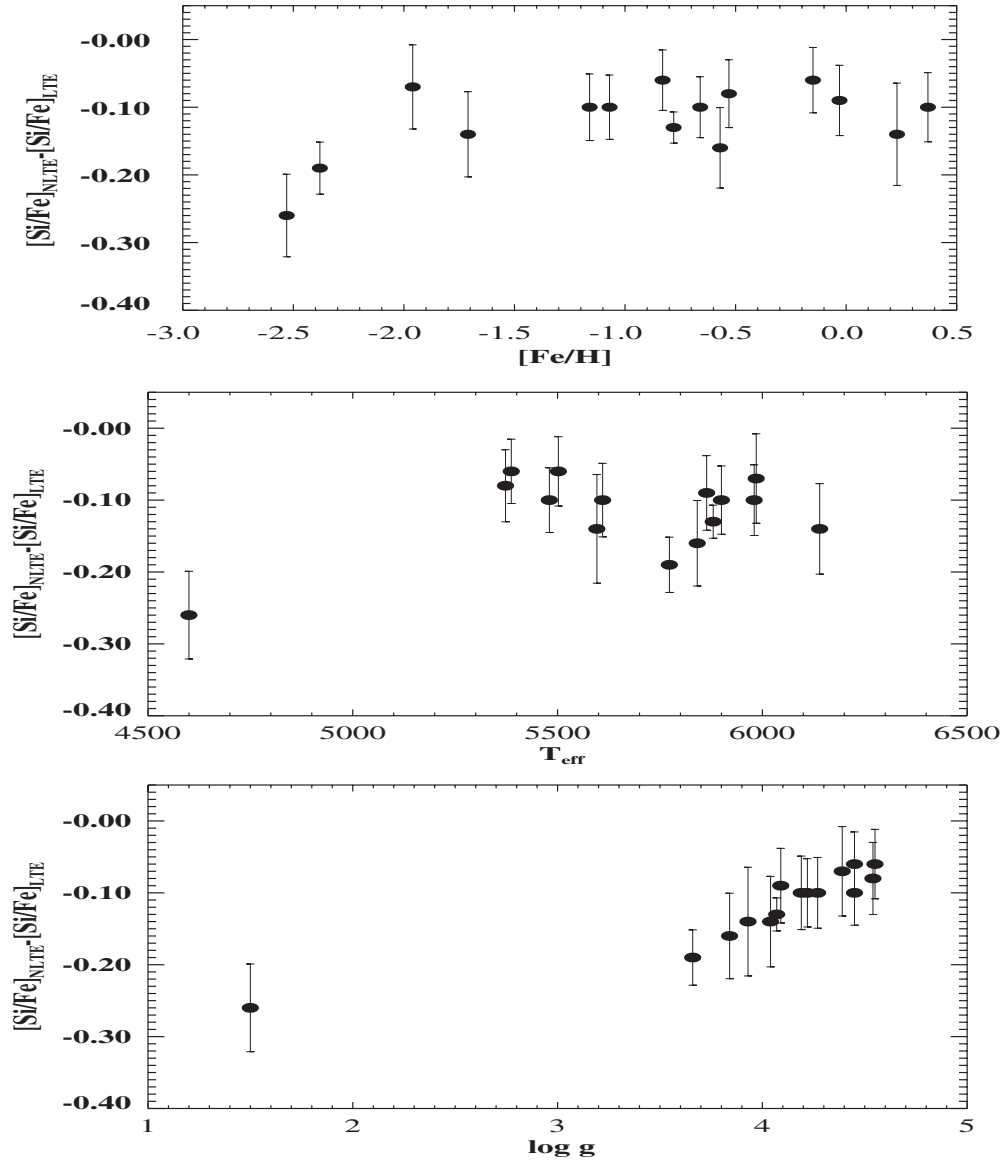
**Figure 3.** Difference of [Si/Fe] abundance ratios calculated under NLTE and LTE assumptions for the two strong Si I lines (10585 and 10827 Å) as a function of (a) metal abundance, (b) temperature, and (c) surface gravity.

**Table 3**
Stellar Silicon LTE and NLTE Abundances Given Relative to the Iron LTE Abundances Derived From the Fe II Lines[a]

| Name | $T_{\rm eff}$ | log $g$ | [Fe/H] | $\xi$ | [Si I $_{\rm LTE}$/Fe] (ir) | [Si I $_{\rm NLTE}$/Fe] (ir) | [Si I $_{\rm LTE}$/Fe] (opt) | [Si I $_{\rm NLTE}$/Fe] (opt) |
|------|------|------|--------|-------|------------------------|-------------------------|------------------------|-------------------------|
| G 29-23 | 6140 | 4.04 | −1.71 | 1.50 | 0.38 ± 0.059 | 0.24 ± 0.022 | 0.07 ± 0.07 | 0.16 ± 0.00 |
| HD 6582 | 5387 | 4.45 | −0.83 | 0.89 | 0.37 ± 0.040 | 0.31 ± 0.020 | 0.26 ± 0.033 | 0.25 ± 0.031 |
| HD 10700 | 5373 | 4.54 | −0.53 | 0.80 | 0.19 ± 0.044 | 0.10 ± 0.024 | 0.18 ± 0.036 | 0.17 ± 0.032 |
| HD 19445 | 5985 | 4.39 | −1.96 | 1.50 | 0.29 ± 0.050 | 0.22 ± 0.037 | 0.16 ± 0.005 | 0.24 ± 0.020 |
| HD 122563 | 4600 | 1.50 | −2.53 | 1.90 | 0.46 ± 0.060 | 0.20 ± 0.011 | 0.22 ± 0.05 | 0.22 ± 0.050 |
| HD 131156 | 5500 | 4.55 | −0.15 | 0.80 | 0.12 ± 0.040 | 0.06 ± 0.027 | 0.05 ± 0.019 | 0.04 ± 0.020 |
| HD 140283 | 5773 | 3.66 | −2.38 | 1.50 | 0.42 ± 0.035 | 0.23 ± 0.016 | 0.17 ± 0.10 | 0.29 ± 0.030 |
| HD 141004 | 5864 | 4.09 | −0.03 | 1.05 | 0.14 ± 0.046 | 0.05 ± 0.024 | 0.06 ± 0.034 | 0.04 ± 0.026 |
| HD 142373 | 5841 | 3.84 | −0.57 | 1.24 | 0.27 ± 0.056 | 0.11 ± 0.020 | 0.14 ± 0.018 | 0.13 ± 0.023 |
| HD 148816 | 5880 | 4.07 | −0.78 | 1.20 | 0.40 ± 0.019 | 0.27 ± 0.013 | 0.25 ± 0.042 | 0.25 ± 0.043 |
| HD 161797 | 5596 | 3.93 | +0.23 | 1.17 | 0.21 ± 0.072 | 0.07 ± 0.023 | 0.10 ± 0.033 | 0.09 ± 0.038 |
| HD 182572 | 5610 | 4.19 | +0.37 | 1.01 | 0.27 ± 0.044 | 0.17 ± 0.026 | 0.12 ± 0.024 | 0.10 ± 0.025 |
| HD 194598 | 5980 | 4.27 | −1.16 | 1.60 | 0.30 ± 0.039 | 0.20 ± 0.030 | 0.24 ± 0.027 | 0.23 ± 0.026 |
| HD 201891 | 5900 | 4.22 | −1.07 | 1.20 | 0.43 ± 0.041 | 0.32 ± 0.024 | 0.27 ± 0.026 | 0.26 ± 0.027 |
| HD 224930 | 5480 | 4.45 | −0.66 | 0.90 | 0.24 ± 0.036 | 0.14 ± 0.027 | 0.13 ± 0.029 | 0.12 ± 0.029 |

**Note.** [a]Our NLTE calculations for Fe I/II based on the advanced atomic model (Mashonkina et al. 2011) support the earlier conclusion of Korn et al. (2003) that the NLTE effects for the Fe II lines are negligible.
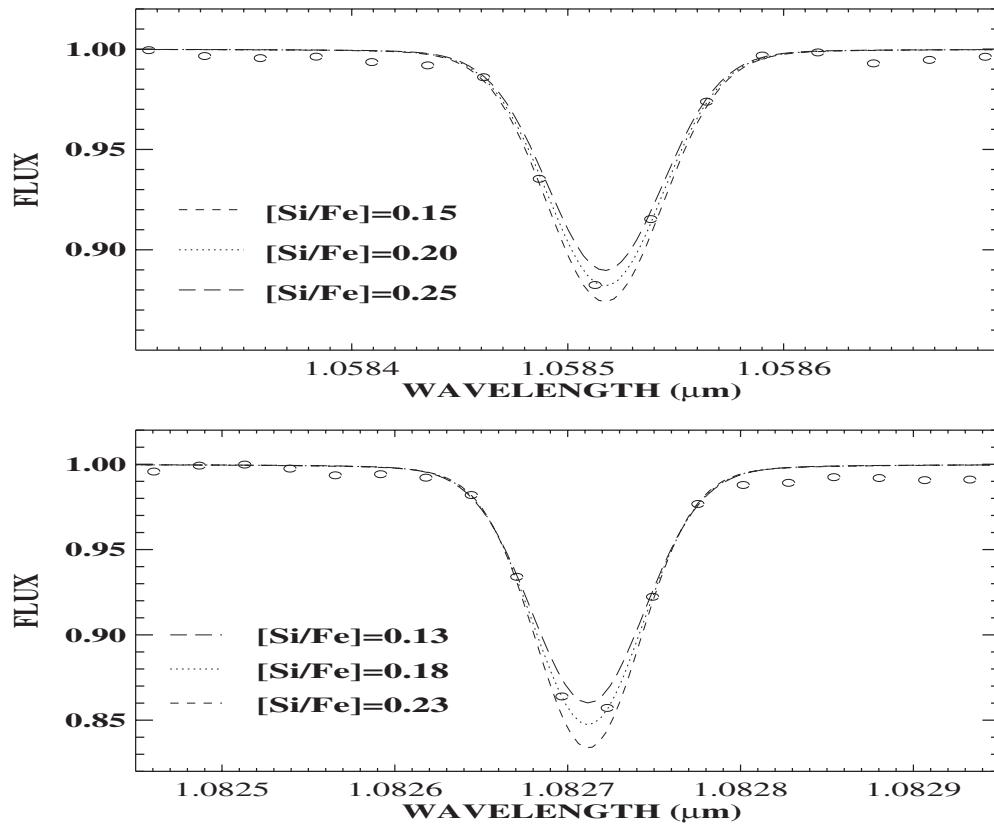
**Figure 4.** Profile fitting of the near-infrared Si I lines in the spectrum of our program stars. The open circles are the observational data, the dotted line is the best-fit synthesis, and the dashed and long dashed lines are synthetic spectra with Si abundances of $\pm 0.05$ dex relative to the best fit.
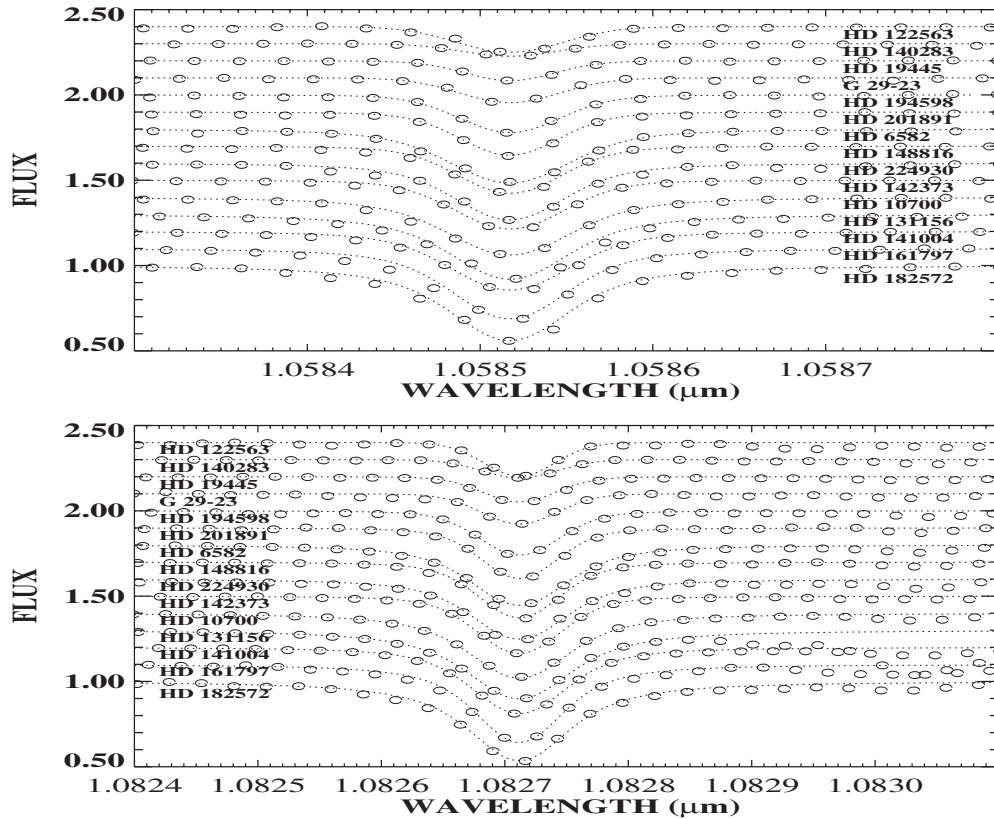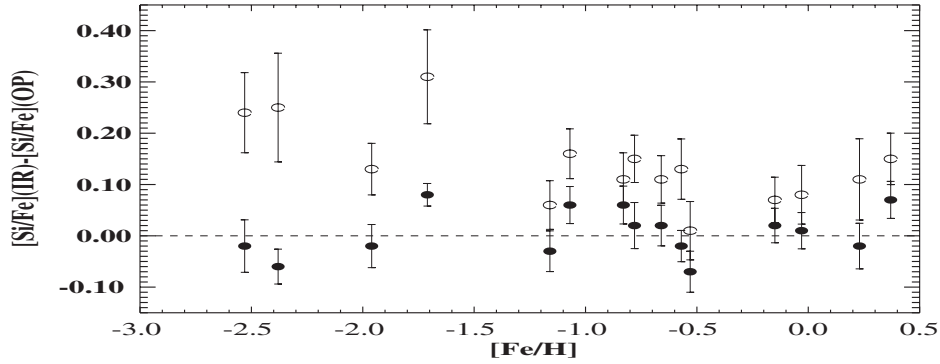


**Figure 5.** Profile fitting of the near-infrared Si I lines in the spectrum of our program stars. Observed spectrum —open circles, NLTE profiles—dotted line.

**Figure 6.** Differences of silicon abundances between the infrared and optical lines. Open circles (○) are LTE results, while filled circles (●) are for NLTE results. It is obvious that the LTE results give a large difference between the Si abundances based on optical and infrared lines.
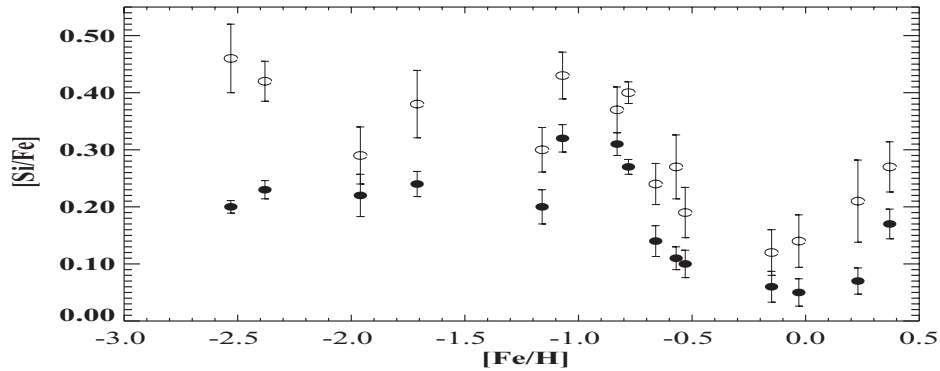


**Figure 7.** Abundance ratios [Si/Fe] as a function of [Fe/H]. Filled circles (●) represent the NLTE results, while open circles (○) are for LTE results. The LTE results overestimate the Si abundances.

terms from the excited ones. The thresholds of the three terms are 1500, 1700, and 2000 Å, respectively (Shi et al. 2008, Figure 2). In this wavelength region, the most important continuous absorption is the free–free quasi-molecular absorption and satellites in Ly$\alpha$ due to collisions with H and $H^+$ (Allard et al. 1998), especially for warm metal-poor stars (see Shi et al. 2009 for details). As already discussed in Shi et al. (2008), there is an unusually large energy gap between the ground state, $3p\,^3P$, the two metastable terms $3p\,^1D$ and $3p\,^1S$, and the first excited levels of neutral silicon. These gaps are about 5, 4, and 3 eV, respectively, and they shift all lines emerging from those levels into the UV, most of them below 2000 Å. Therefore, the interaction of the three most populated Si I levels with the Si II ion is completely based on bound–free processes, where photoionization and ionization by electron collisions compete in strength. Due to the large photoinization cross-sections for the three lowest levels, the departure coefficients of Si I are very sensitive to the UV radiation field. When the Ly$\alpha$ continuum absorption is not included, the extreme underpopulation of Si I levels in the atmospheres of warm metal-poor stars is clearly seen (see Shi et al. 2009, Figure 5).

The abundance analyses of Si I infrared lines clearly show the NLTE effects. It should be noted that the NLTE effects differ from line to line—the strong 10585 and 10827 Å lines show large NLTE effects for our program stars, while the weak lines show the smallest NLTE abundance effects (<0.02 dex, Table 2). The abundance differences between the LTE and NLTE analyses for the two strong Si I lines at 10585 and 10827 Å are plotted in Figure 3 as a function of metal abundance, temperature, and surface gravity, respectively. The NLTE effects increase with decreasing surface gravity. However, it should be

noted that we only include one giant star (HD 122563) in our sample, and that this trend should be confirmed by more sample stars.

The important uncertainties of the NLTE effects are due to the lack of suitable cross-section data for collisional excitation and ionization by electrons and hydrogen. Of the two, the treatment of the hydrogen collision is the most uncertain. Hydrogen collisions are important and may well dominate the collision rates in hot metal-poor stars (Asplund 2005). Only limited information on selected transitions in a few elements has so far been gained from laboratory measurements and detailed quantum-mechanical calculations. Those results show that the Drawin formula overestimates the inelastic hydrogen collisional cross-sections by one to six orders of magnitude (Belyaev et al. 1999; Belyaev & Barklem 2003; Barklem et al. 2012). We apply a scaling factor $S_H$ to the Drawin formula and calibrate it based on solar stellar observations. Fortunately, for Si, as we already discussed in Section 4.1, we can determine the $S_H$ scale from the fitting of the strong solar infrared lines. Thus, we estimate that the uncertainties in the NLTE corrections are less than 0.1 dex.

## 5. RESULTS

### 5.1. Stellar Silicon Abundances

The abundance determinations for our program stars are made using spectral synthesis. Some examples of the profile fitting are presented in Figures 4 and 5. Consistent abundance results are obtained between different lines when NLTE effects are included; the final abundance scatter of single lines is between 0.01 and 0.12 for our program stars, while the scatter can reach to 0.3 dex for the extreme case under the LTE situation (see

Table 2 for details). The derived abundance results based on both the infrared and optical lines are presented in Table 3.

### 5.2. Comparison with the Optical Results

We have also been determined the silicon abundances from the optical lines based on LTE and NLTE analyses for these stars (Shi et al. 2009, 2011; J. Li et al. 2012, in preparation). In Figure 6, we compare the [Si/Fe] values determined from infrared and optical lines for our program stars. A comparison of the abundances shows that consistent results are obtained when the NLTE effects are included—the differences are less than 0.1 dex for all program stars—while differences as large as 0.2 dex can be found for the LTE results in some cases.

### 6. DISCUSSION AND CONCLUSIONS

We have determined silicon abundances for 15 nearby stars, spanning the range $-2.6 <$ [Fe/H] $< \sim 0.4$, based on the infrared lines. All abundances are derived from NLTE statistical equilibrium calculations. Figure 7 displays the behavior of the [Si/Fe] ratio with the metal abundance for all stars considered in this paper. Based on our results, we come to the following conclusions.

1. Silicon is overabundant by 0.2–0.3 dex for metal-poor stars, and the LTE results overestimate the Si abundances.
2. The NLTE effects vary with different infrared lines. The weak lines are insensitive to NLTE effects, while the strong lines show large NLTE effects. NLTE leads to enhanced absorption in the line cores and negative abundance corrections over the range of stellar parameters studied here. This effect may depend on the surface gravity, and thus tend to be large for giant stars.
3. Our results show that NLTE largely removes obvious discrepancies between optical and infrared lines obtained under an LTE assumption.

   Thus, it is important to consider the NLTE effects when the silicon abundances are determined using the infrared lines.

## REFERENCES

Allard, N. F., Drira, I., Gerbaldi, M., Koester, D., & Spielfiedel, A. 1998, A&A, 335, 1124
Ali, A. W., & Griem, H. R. 1966, Phys. Rev., 144, 366
Allen, C. W. 1973, Astrophysical Quantities (3rd ed.; London: Athlone)
Anders, E., & Grevesse, N. 1989, Geochim. Cosmochim. Acta, 53, 197
Anstee, S. D., & O'Mara, B. J. 1991, MNRAS, 253, 549
Anstee, S. D., & O'Mara, B. J. 1995, MNRAS, 276, 859
Asplund, M. 2005, ARA&A, 43, 381
Barklem, P. S., Belyaev, A. K., Spielfiedel, A., Guitou, M., & Feautrier, N. 2012, A&A, 541, A80
Barklem, P. S., Piskunov, N., & O'Mara, B. J. 2000, A&AS, 142, 467
Belyaev, A. K., & Barklem, P. S. 2003, Phys. Rev. A, 68, 62703
Belyaev, A. K., Grosser, J, Hahne, J, & Menzel, T. 1999, Phys. Rev. A, 60, 2151
Butler, K., & Giddings, J. 1985, Newsletter on the Analysis of Astronomical Spectra No. 9, Univ. London
Dekker, H., Dódorico, S., Kaufer, A., Delabre, B., & Kotzlowski, H. 2000, Proc. SPIE, 4008, 534
Drawin, H. W. 1968, Z. Phys., 211, 404
Drawin, H. W. 1969, Z. Phys., 225, 483
Fuhrmann, K., Axer, M., & Gehren, T. 1993, A&A, 271, 451
Fuhrmann, K., Pfeiffer, M., Frank, C., et al. 1997, A&A, 323, 909
Gehren, T., Butler, K., Mashonkina, L., Reetz, J., & Shi, J. R. 2001, A&A, 366, 981
Gehren, T., Liang, Y. C., Shi, J. R., Zhang, H. W., & Zhao, G. 2004, A&A, 413, 1045
Gehren, T., Shi, J. R., Zhang, H. W., Zhao, G., & Korn, A. J. 2006, A&A, 451, 1065
Grupp, F. 2004, A&A, 420, 289
Iwamoto, K., Brachwitz, F., Nomoto, K., et al. 1999, ApJS, 125, 439
Jönsson, H., Ryde, N., Nissen, P. E., et al. 2011, A&A, 530, 144
Kobayashi, N., Tokunaga, A. T., Terada, H., et al. 2000, Proc. SPIE, 4008, 1056
Korn, A., Shi, J. R., & Gehren, T. 2003, A&A, 407, 691
Kurucz, R. L. 1979, ApJS, 40, 1
Kurucz, R. L. 1992, RevMexAA, 23, 45
Maeda, K., Röpke, F. K., Fink, M., et al. 2010, ApJ, 712, 624
Mashonkina, L., Gehren, T., Shi, J. R., Korn, A., & Gruup, F. 2011, A&A, 528, A87
Nahar, S. N., & Pradhan, A. K. 1993, J. Phys. B: At. Mol. Opt. Phys., 26, 1109
Ohkubo, T., Umeda, H., Maeda, K., et al. 2006, ApJ, 645, 1352
Seaton, M. J. 1962, in Atomic and Molecular Processes, ed. D. R. Bates (New York: Academic), 374
Seaton, M. J., Mihalas, D., & Pradhan, A. K. 1994, MNRAS, 266, 805
Shi, J. R., Gehren, T., Butler, K., Mashonkina, L., & Zhao, G. 2008, A&A, 486, 303
Shi, J. R., Gehren, T., Mashonkina, L., & Zhao, G. 2009, A&A, 503, 533
Shi, J. R., Gehren, T., & Zhao, G. 2004, A&A, 423, 683
Shi, J. R., Gehren, T., & Zhao, G. 2011, A&A, 534, A103
Steenbock, W., & Holweger, H. 1984, A&A, 130, 319
Takeda, Y., & Takada-Hidai, M. 2011a, PASJ, 63, 537
Takeda, Y., & Takada-Hidai, M. 2011b, PASJ, 63, 547
Thielemann, F. K., Argast, D., Brachwitz, F., et al. 2002, ApSS, 281, 25
Tokunaga, A. T., Kobayashi, N., Bell, J., et al. 1998, Proc. SPIE, 3354, 512
Tsujimoto, T., Nomoto, K., Yoshii, Y., et al. 1995, MNRAS, 277, 945
van Regemorter, H. 1962, ApJ, 136, 906
Woosley, S. E., & Weaver, T. A. 1995, ApJS, 101, 181
Zhao, G., Butler, K., & Gehren, T. 1998, A&A, 333, 219